

NUMERICAL VERIFICATION OF THE RELATIONSHIP BETWEEN THE "IN-PLANE GEOMETRIC CONSTRAINTS" USED IN FRACTURE MECHANICS PROBLEMS

Marcin GRABA*

*Kielce University of Technology, Faculty of Mechatronics and Machine Design, Al. 1000-lecia PP 7, 25-314 Kielce, Poland

mgraba@tu.kielce.pl

Abstract: In the paper, numerical verification and catalogue of the numerical solutions based on Modify Boundary Layer Approach to determine the relationship between Q-stress and T-stress are presented. Based on the method proposed by Larsson and Carlsson, the Q-stress value are calculated for some elastic-plastic materials for different value of T-stress and external load expressed by J-integral. The influence of the external load, T-stress value and material properties on Q-stress value were tested. Such catalogue may be useful during solving the engineering problems, especially while is needed to determine real fracture toughness with including the geometric constraints, what was proposed in FITNET procedures.

Key words: Fracture, Crack, Stress Fields, HRR, MBLA, in-Plane Constraints, Q-Stress, T-Stress.

1. DESCRIPTION OF THE STRESS FIELD NEAR CRACK TIP – THEORETICAL BACKGROUNDS

For mode I of loading, stress field ahead of a crack tip in elastic linear isotropic material can be given by (Williams, 1957):

$$\begin{aligned} \sigma_{11} = \sigma_{xx} &= \frac{K_I}{\sqrt{2\pi r}} \left[\cos \frac{\theta}{2} \left(1 - \sin \frac{\theta}{2} \sin \frac{3\theta}{2} \right) \right], \\ \sigma_{22} = \sigma_{yy} &= \frac{K_I}{\sqrt{2\pi r}} \left[\cos \frac{\theta}{2} \left(1 + \sin \frac{\theta}{2} \sin \frac{3\theta}{2} \right) \right], \\ \sigma_{12} = \tau_{xy} &= \frac{K_I}{\sqrt{2\pi r}} \left[\cos \frac{\theta}{2} \sin \frac{\theta}{2} \cos \frac{3\theta}{2} \right], \\ \sigma_{33} = \sigma_{zz} &= 0 \quad \text{for plane stress,} \\ \sigma_{33} = \sigma_{zz} &= \nu(\sigma_{xx} + \sigma_{yy}) \quad \text{for plane strain,} \end{aligned} \quad (1)$$

where σ_{ij} is the stress tensor, r and θ are as defined in Fig. 1, ν is Poisson's ratio, K_I is the Stress Intensity Factor (SIF).

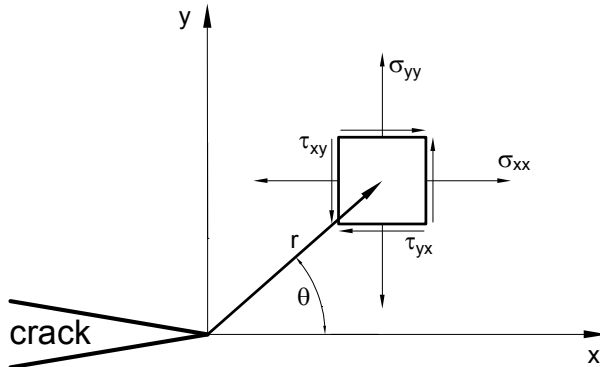


Fig. 1. Definition of the coordinate axis ahead of a crack tip
The z direction is normal to the page
(own Fig. based on (Williams, 1957))

The SIF defines the amplitude of the crack tip singularity. That is, stresses near the crack tip increase in proportion to K . Moreover, the stress intensity factor completely defines the crack tip conditions; if K is known, it is possible to solve for all components of stress, strain, and displacement as a function of r and θ .

This single-parameter description of crack tip conditions turns out to be one of the most important concepts in fracture mechanics (Williams, 1957).

In 1968, Hutchinson (1968) and Rice and Rosengren (1968) derived the singular stress-strain fields at a crack tip in a power-law hardening material (which called the HRR-field). The hardening law used by Hutchinson and Rice and Rosengren is given by:

$$\frac{\varepsilon}{\varepsilon_0} = \alpha \left(\frac{\sigma}{\sigma_0} \right)^n, \quad (2)$$

where σ_0 is a reference stress value that is usually equal to the yield strength, $\varepsilon_0 = \sigma_0/E$, α is a dimensionless constant, and n is the strain hardening exponent.

Assuming the Ramberg-Osgood material, the results obtained by Hutchinson and Rice and Rosengren for plane strain and for plane stress may be expressed in the following form:

$$\sigma_{ij} = \sigma_0 \left(\frac{J}{\alpha \sigma_0 \varepsilon_0 I_n r} \right)^{\frac{1}{1+n}} \tilde{\sigma}_{ij}(\theta, n), \quad (3)$$

$$\varepsilon_{ij} = \alpha \varepsilon_0 \left(\frac{J}{\alpha \sigma_0 \varepsilon_0 I_n r} \right)^{\frac{n}{1+n}} \tilde{\varepsilon}_{ij}(\theta, n), \quad (4)$$

where J is the J -integral, I_n is an integration constant that depends on n , $\tilde{\sigma}_{ij}(\theta, n)$ and $\tilde{\varepsilon}_{ij}(\theta, n)$ are dimensionless functions of n and θ . These parameters also depend on the stress state (i.e. plane stress or plane strain). All this function may be determined using the algorithm and computer program presented by Galkiewicz and Graba (2006).

The J -integral defines the amplitude of the HRR singularity, just as the stress intensity factor characterizes the amplitude of the linear elastic singularity. Thus, J -integral completely describes the conditions within the plastic zone. A structure in small-scale yielding has two singularity-dominated zones: one in the elastic region, where stress varies as $1/\sqrt{r}$ and one in the plastic zone where stress varies as $(1/r)^{1/(1+n)}$. The latter often persists long after the linear elastic singularity zone has been destroyed by crack tip plasticity.

The HRR singularity contains the same apparent anomaly as the linear elastic fracture mechanics singularity; namely, both predict infinite stresses as $r \rightarrow 0$. The singular field does not persist all the way to the crack tip, however. The large strains at the crack tip cause the crack to blunt, which reduces the stress triaxiality locally. The blunted crack tip is a free surface; thus σ_{xx} must vanish at $r = 0$.

The analysis that leads to the HRR singularity doesn't consider the effect of the blunted crack tip on the stress fields, nor does it take account of the large strains that are present near the crack tip. This analysis is based on small strain theory, which is the multi-axial equivalent of engineering strain in a tensile test. Small strain theory breaks down when strains are greater than about 10%.

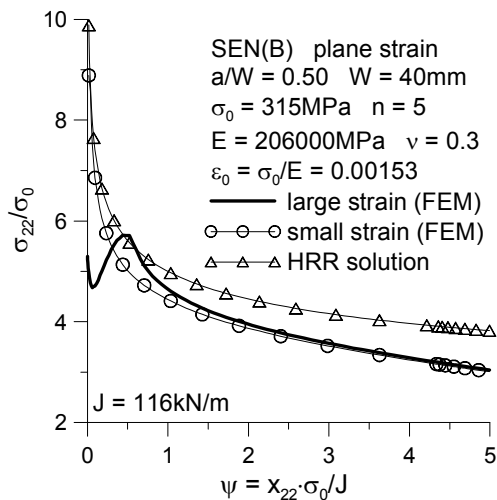


Fig. 2. The stress distribution near a crack tip (curves were obtained using the FEM for small and finite strain and HRR formula)

McMeeking and Parks (1979) performed crack tip finite element analyses that incorporated large strain theory and finite geometry changes. Some of their results are shown in Fig. 2, which is a plot of stress normal to the crack plane versus distance. The HRR singularity is also shown on this plot. Note that both axes are dimensionless in such a way that both curves are invariant, as long as the plastic zone is small compared to specimen dimensions. The solid curve in Fig. 2 reaches a peak when the ratio $x \cdot \sigma_0 / J$ is approximately unity, and decreases as $x \rightarrow 0$. This distance corresponds approximately to twice the Crack Tip Opening Displacement (CTOD). The HRR singularity is invalid within this region, where the stresses are influenced by large strains and crack blunting.

Presented above solutions for stress (Eq. (1) for linear fracture mechanics and Eq. (3) for nonlinear fracture mechanics) only describe the near tip field and consider only the first term of Taylor expansion. In the linear case, the second term in the Taylor expansion corresponds to the so called T -stress which acts in the

direction parallel to the crack advance direction. The mode I stress field becomes:

$$\sigma_{ij} = \frac{K_I}{\sqrt{2\pi r}} f_{ij}(\theta) + \begin{bmatrix} T & 0 & 0 \\ 0 & 0 & 0 \\ 0 & 0 & \nu T \end{bmatrix}, \quad (5)$$

here T is a uniform stress in the x direction (which induces a stress νT in the z direction in plane strain).

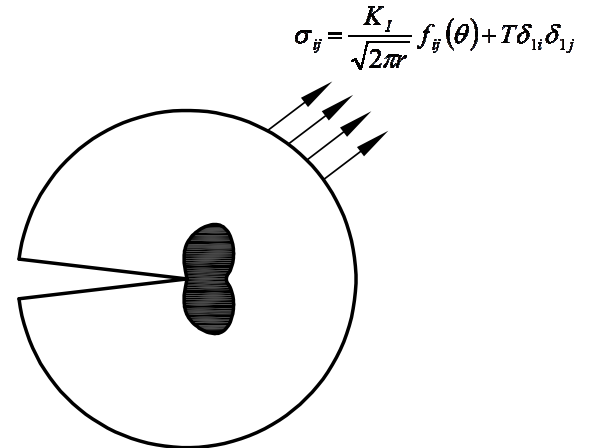


Fig. 3. Modified boundary layer analysis. The first two terms of the Williams series are applied as boundary conditions (own Fig. based on Anderson, (1995))

The more common form of Eq. (9) is the following entry:

$$\sigma_{ij} = \frac{K_I}{\sqrt{2\pi r}} f_{ij}(\theta) + T \delta_{ij} \delta_{ij}, \quad (6)$$

where δ_{ij} is the Kronecker delta.

We can assess the influence of the T stress by constructing a circular model that contains a crack, as illustrated in Fig. 3. On the boundary of this model, let us apply in-plane tractions that correspond to Eq. (5). A plastic zone develops at the crack tip, but its size must be small relative to the size of the model in order to ensure the validity of the boundary conditions, which are inferred from an elastic solution. This configuration, often referred to as a modified boundary layer analysis, simulates the near tip conditions in an arbitrary geometry, provided the plasticity is well contained within the body.

Fig. 4 is a plot of finite element results from a modified boundary layer analysis (Neimitz et al., 2007) that show the effect of the T stress on stresses deep inside the plastic zone, obtained for large strain assumption. The special case of $T=0$ corresponds to the small-scale yielding limit, where the plastic zone is a negligible fraction of the crack length and size of the body, and the singular term uniquely defines the near-tip fields. The single-parameter description is rigorously correct only for $T=0$. Note that negative T values cause a significant downward shift in the stress fields. Positive T values shift the stresses to above the small-scale yielding limit, but the effect is much less pronounced than it is for negative T stress.

Note that the HRR solution does not match the $T=0$ case. The stresses deep inside the plastic zone can be represented by a power series, where the HRR solution is the leading term. Fig. 4 indicates that the higher order plastic terms are not negligible when $T=0$.

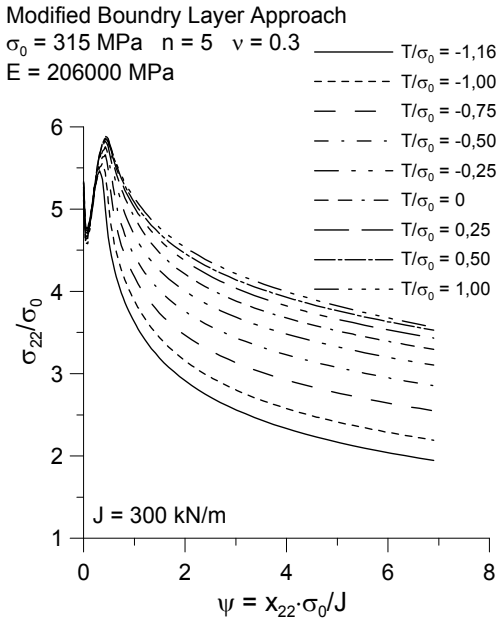


Fig. 4. The stress distribution in front of the crack, computed using modified boundary layer approach for constant SIF, K_I , and changing T -stress. Properties of material like in the Sumpter and Forbes paper (Sumpter and Forbes, 1992)

In a cracked body subject to Mode I loading, the T stress, like K_I , scales with the applied load. The biaxiality ratio relates T to stress intensity:

$$\beta = \frac{T\sqrt{\pi a}}{K_I}, \quad (7)$$

where a is the crack length.

For a through-thickness crack in an infinite plate subject to a remote normal stress $\beta = -1$. Thus a remote stress induces a T stress of $-\sigma$ in the x direction.

In the nonlinear fracture mechanics, the Q factor was introduced by O'Dowd and Shih (1991, 1992) to account for difference between the HRR field and finite element results. The Q factor (also called Q -stress) corresponds to an additional hydrostatic pressure. The modified by O'Dowd and Shih stress field is obtained as:

$$\sigma_{ij} = (\sigma_{ij})_{HRR} + Q\sigma_0\delta_{ij}, \quad (8)$$

where $(\sigma_{ij})_{HRR}$ is given by Eq. (3).

For small scale yielding, Eq. (8) can be written in the following form:

$$\sigma_{ij} = (\sigma_{ij})_{T=0} + Q\sigma_0\delta_{ij}. \quad (9)$$

The Q parameter can be inferred by subtracting the stress field for the $T=0$ reference state from the stress field of interest. O'Dowd and Shih and most subsequent researchers defined Q as follows:

$$Q = \frac{(\sigma_{yy}) - (\sigma_{yy})_{T=0}}{\sigma_0} \text{ for } \theta=0 \text{ and } \frac{r\sigma_0}{J} = 2. \quad (10)$$

Referring to Fig. 4, we see that Q is negative when T is negative. For the modified boundary layer solution, T and Q are uniquely related.

Fig. 5 is a plot of Q versus T for a two work hardening exponents. A relation between Q and T stress, based on numerical calculations, using large strain theory and incremental strain plasticity is given by O'Dowd and Shih (1991) as:

$$Q \approx a_0 + a_1(T/\sigma_0) + a_2(T/\sigma_0)^2 + a_3(T/\sigma_0)^3, \quad (11)$$

where coefficients a_0 , a_1 , a_2 and a_3 were given only for two work hardening exponents: for $n=5$: $a_0=-0.10$, $a_1=0.76$, $a_2=-0.32$, $a_3=-0.01$ and for $n=10$: $a_0=-0.10$; $a_1=0.76$, $a_2=-0.52$, $a_3=0$. Proposed by Eq. (11) relationship is the result of the matching mathematical formula to numerical results.

In 1995 O'Dowd (O'Dowd, 1995) was proposed, to describe the relationship between Q and T stress by linear formula, as

$$Q = \begin{cases} T/\sigma_0 & \text{for } T/\sigma_0 < 0 \\ 0.5 \cdot T/\sigma_0 & \text{for } T/\sigma_0 > 0 \end{cases}. \quad (12)$$

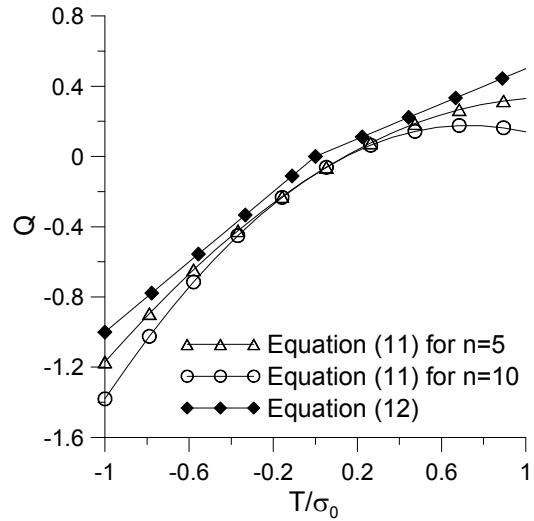


Fig. 5. Relationship between Q and T stress, based on Equations (11) and (12) (based on O'Dowd and Shih (1991))

Fig. 5 shows graphically the mutual relationship between the Q and T stress, based on formulas (11) and (12). The use of both dependencies is relatively simple. In the case of formula (11) must know the values of the coefficients a_0 , a_1 , a_2 and a_3 . Seems to be easier to use formula (12), because it is required only knowledge level of T stress, which for various geometries can be found in the literature (Sherry et al., 1991), (Leevers and Radon, 1983).

When Equation (12) will be used in analysis of the real structural element, as can be observed, this formula did not take into account the geometry characterization, for example material properties, external load, kind of specimen. Formula (12), takes into account only crack length, because, T stress depend on relative crack length (Leevers and Radon, 1983).

However, thanks to its simplicity, Equation (12) has found use in the solving engineering problems and it was recommended by FITNET procedures (FITNET, 2006). It should be noted that both Equations - (11) and (12) were based on analysis of small scale yielding, based on Modify Boundary Layer Approach (MBLA).

It should be noted also that both Equations generally do not include external load, which in the case of plane strain strongly affects the Q stress level.

2. UTILIZATION OF THE CONSTRAINT PARAMETERS IN THE EVALUATION OF FRACTURE TOUGHNESS

Both constraint parameters, the Q and T stress were found application in European Engineering Programs, like SINTAP (SINTAP, 1999) and FITNET (FITNET, 2006). The Q -stress or T -stress is applied under construction of the fracture criterion and to assessment the fracture toughness of the structural component. Real fracture toughness K_{mat}^C , may be evaluated using the formula proposed by Ainsworth and O'Dowd (1994). Ainsworth and O'Dowd have shown that the increase in fracture in both the brittle and ductile regimes may be represented by an expression of the form:

$$K_{mat}^C = \begin{cases} K_{mat} & \beta L_r > 0 \\ K_{mat} [1 + \alpha(-\beta L_r)^k] & \beta L_r < 0 \end{cases} \quad (13)$$

where K_{mat} is the fracture toughness for plane strain condition obtained using FITNET procedures, and β is the parameter calculated using following formula:

$$\beta = \begin{cases} T/(L_r \sigma_0), & \text{for elastic materials,} \\ Q/L_r, & \text{for elastic-plastic materials,} \end{cases} \quad (14)$$

where L_r is the ratio of the actual external load P and the limit load P_0 (or the reference stress), which may be calculated using FITNET procedures (FITNET, 2006).

The constants α and k which are occurring in Eq. (13), are material and temperature dependent (Tab. 1). Sherry and et al., (2005a, b) proposed the designation procedures to calculate the constants α and k . Thus J - Q and K - T theories have practical application in engineering issues.

Tab 1. Some values of the α and k parameters, which are occurring in Eq. (13) (SINTAP, 1999; FITNET, 2006)

material	temperature	fracture mode	α	k
A533B (steel)	-75°C	cleavage	1.0	1.0
A533B (steel)	-90°C	cleavage	1.1	1.0
A533B (steel)	-45°C	cleavage	1.3	1.0
Low Carbon Steel	-50°C	cleavage	1.3	2.0
A515 (steel)	+20°C	cleavage	1.5	1.0
ASTM 710 Grade A	+20°C	ductile	0.0	1.0
			0.6	1.0
			1.0	2.0

The reciprocal relationship between "in-plane constraint" parameters, for what can be considered the Q -stress and T -stress may be very useful in practical engineering problems, to determination of the real fracture toughness or in failure assessment diagrams (FAD) analysis when correction of the FAD curve using constraint parameter is done (SINTAP, 1999), (FITNET, 2006).

Thus, in this paper, catalogue of the Q - T trajectories obtained using MBLA analysis will be presented. The influence of the material properties will be tested.

3. DETAILS OF THE NUMERICAL ANALYSIS

In the numerical analysis, ADINA System 8.5.4 (ADINA, 2008a, b) was used. Computations were performed for plane strain using small strain option and the Modify Boundary Layer Approach (MBLA) model. The MBLA model consists of big circle, which radius around the crack tip where the boundary conditions are modeled is 10 meters long. Due to the symmetry, only a half of the circle was modeled (see Fig. 6). The boundary conditions are modeled using the following relationship:

$$\begin{cases} u_1 = \frac{K}{E} (1+\nu) \sqrt{\frac{r}{2\pi}} \cos\left(\frac{\theta}{2}\right) \left[\kappa - 1 + 2 \sin^2\left(\frac{\theta}{2}\right) \right] + \\ + (1-\nu^2) \frac{T}{E} r \cos(\theta) \\ u_2 = \frac{K}{E} (1+\nu) \sqrt{\frac{r}{2\pi}} \sin\left(\frac{\theta}{2}\right) \left[\kappa + 1 - 2 \cos^2\left(\frac{\theta}{2}\right) \right] + \\ - \nu(1+\nu) \frac{T}{E} r \sin(\theta) \end{cases}, \quad (15)$$

where K is the stress intensity factor (SIF) calculated from J -integral value using formula $K = \sqrt{JE/(1-\nu^2)}$ – in presented in the paper numerical program the following values of the J -integral were tested: $J=\{10, 25, 50, 100, 250, 500\}$ kN/m; r and θ are polar coordinates; ν is the Poisson's ratio; E is Young's modulus; T is the T stress expressed in stress unit ($T \cdot \sigma$) – in presented in the paper numerical program, the following values of the T parameter were tested: $T=\{0.5, 0.25, 0, -0.25, -0.5, -1\}$; $\kappa=3-4\nu$ for plane strain; $\kappa=(3-\nu)/(1+\nu)$ for plane stress.

The radius of the crack front was equal to $r_w=5 \cdot 10^{-6}$ m. The crack tip was modeled as half of arc. The crack tip region about to $5 \cdot 10^{-4}$ m was divide into 50 semicircles. The first of them, was at least 20 times smaller then the last one. The finite element mesh was filled with the 9-node plane strain elements. The size of the finite elements in the radial direction was decreasing towards the crack tip, while in the angular direction the size of each element was kept constant. It varied from $\Delta\theta=\pi/19$ to $\Delta\theta=\pi/30$ for various cases tested.

The whole MBLA model was modeled using 2584 finite elements and 10647 nodes. The example finite element model for MBLA analysis is presented in Fig. 6.

In the FEM simulation, the deformation theory of plasticity and the von Misses yield criterion were adopted. In the model the stress-strain curve was approximated by the relation:

$$\frac{\varepsilon}{\varepsilon_0} = \begin{cases} \sigma/\sigma_0 & \text{for } \sigma \leq \sigma_0 \\ \alpha(\sigma/\sigma_0)^n & \text{for } \sigma > \sigma_0 \end{cases}, \quad \text{where } \alpha \neq 1. \quad (16)$$

The tensile properties for the materials which were used in the numerical analysis are presented below in Tab. 2. In the FEM analysis, calculations were done for sixteen material configurations, which were differed by yield stress and the work hardening exponent.

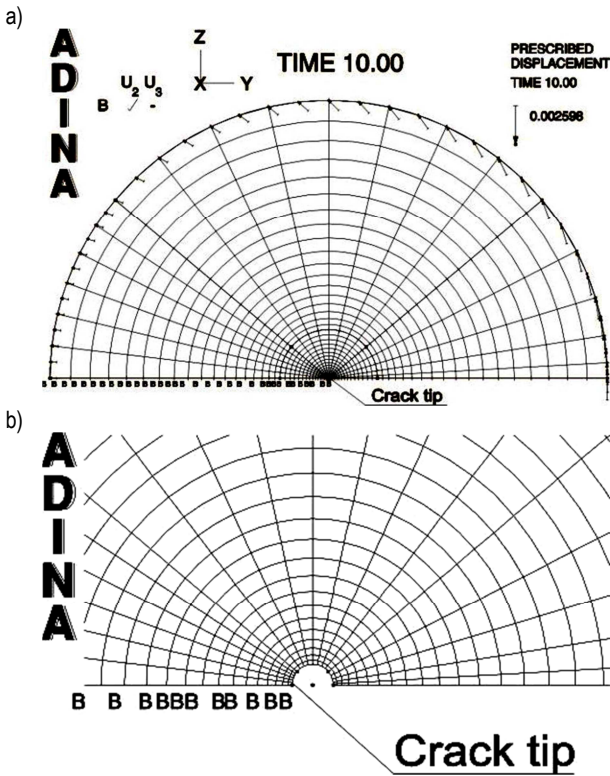


Fig. 6. The MBLA model which was used in the numerical program a) Crack tip region using in the MBLA model b)

The J -integral were calculated using two methods. The first method, called the "virtual shift method", uses concept of the virtual crack growth to compute the virtual energy change. The second method is based on the J -integral definition:

$$J = \int_C [w dx_2 - \mathbf{t}(\partial \mathbf{u} / \partial x_1) ds], \quad (17)$$

where w is the strain energy density, \mathbf{t} is the stress vector acting on the contour C drawn around the crack tip, \mathbf{u} denotes displacement vector and ds is the infinitesimal segment of contour C .

Tab. 2. The mechanical properties of the materials used in numerical analysis and the HRR parameters for plane strain

σ_0 [MPa]	E [MPa]	ν	$\varepsilon_0 = \sigma_0 / E$	α	n	$\bar{\sigma}_{\theta\theta}(\theta = 0)$	l_n
315	206000	0.3	0.00153	1	3	1.94	5.51
500			0.00243		5	2.22	5.02
1000			0.00485		10	2.50	4.54
1500			0.00728		20	2.68	4.21

4. RESULTS OF THE NUMERICAL ANALYSIS

Fig. 7 presents the influence of the T stress parameter value on the shape and size (denoted in Fig. as r_p) of the plastic zone near crack tip. For smaller value of the T stress parameter, the greater plastic zone is observed, if the same level of the J -integral was used to calculate the boundary conditions and the same material characteristic was established. The bigger plastic zone is observed for MBLA model characterized by smaller yield stress (see Fig. 8).

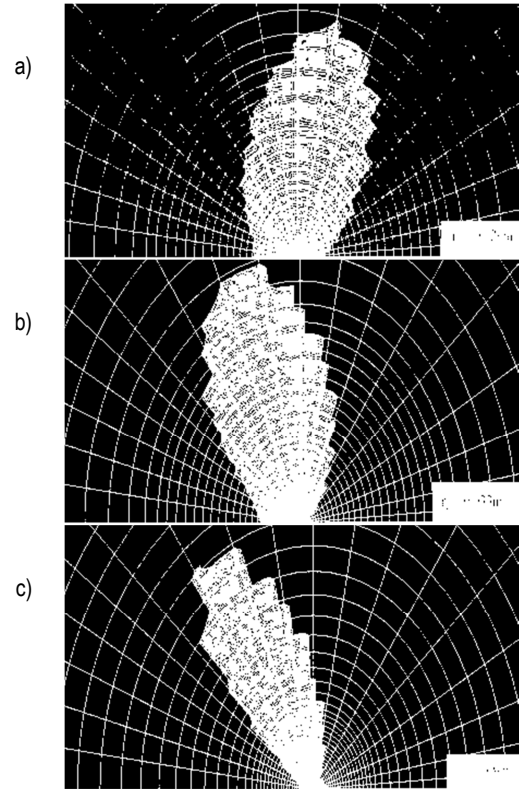


Fig. 7. Influence of the T stress parameter on shape and size of the plastic zone for MBLA model characterized by $\sigma_0=315$ MPa, $n=10$, $J=100$ kN/m: a) $T=0.5$, $r_p=0.029$ m; b) $T=0$, $r_p=0.033$ m; c) $T=-0.5$, $r_p=0.090$ m (brighter region is the plastic zone)

For smaller values of the T stress parameter the, smaller value of the Q stress are observed. The influence of the work hardening exponent on $Q=Q(T)$ trajectories should be considered for a number of configurations. For the cases characterized by yield stress $\sigma_0 \geq 500$ MPa and for J -integral values between 10 and 25kN/m (which are used to determine the boundary conditions), the lower values of the Q stress are observed for weakly strengthen materials (see Fig. 9). For theses cases almost parallel arrangement of the $Q=Q(T)$ trajectories is observed. The highest on the chart are situated curves for strongly strengthen material ($n=3$).

In other cases, when the J -integral value is equal to or greater than 50kN/m, it can be seen the intersecting of the $Q=Q(T)$ curves for different values of the work hardening exponent (see Fig. 10). For small values of the T stress parameter (which means that we are dealing with a case of high-level of the flat geometric constraints), the lower values of Q parameter are observed for weakly hardening materials. Increase value of the T stress parameter makes cutting curves and the reversal of the trend on the chart - then a smaller values of the Q parameter are observed for the case of the strongly hardening materials.

Numerical analysis shown, that the influence of the yield stress on $Q=Q(T)$ trajectories is quite complex. For small values of the J -integral ($J=10$ kN/m or $J=25$ kN/m), it can be concluded, that $Q=Q(T)$ curves characterized by regularity of arrangement, especially for strong hardening materials ($n=3$ and $n=5$). The lowest on the charts are arranged the $Q=Q(T)$ curves, described by small value of the yield stress. This means that for the materials characterized by higher yield stress, the higher values of the Q parameter are obtained (see Fig. 11).

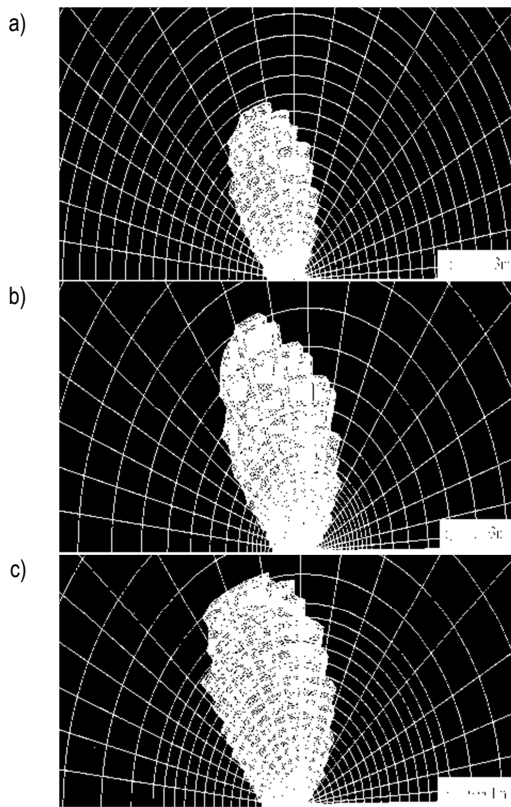


Fig. 8. Influence of the yield stress on shape and size of the plastic zone for MBLA model characterized by $T=0$, $n=10$, $J=100\text{kN/m}$:
 a) $\sigma_0=500\text{MPa}$, $r_p=0.013\text{m}$; b) $\sigma_0=1000\text{MPa}$, $r_p=0.003\text{m}$;
 c) $\sigma_0=1500\text{MPa}$, $r_p=0.001\text{m}$ (brighter region is the plastic zone)

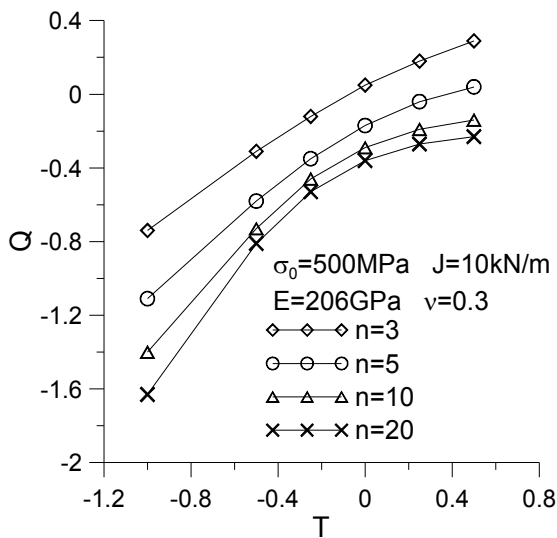


Fig. 9. The influence of the work hardening exponent on the $Q=Q(T)$ trajectories for MBLA characterized by $\sigma_0=500\text{MPa}$, $J=10\text{kN/m}$

The influence of the yield stress on $Q=Q(T)$ trajectories is significant for the low level of the J -integral which was used to determination of the boundary conditions. Sometimes the influence of the yield stress on Q stress value is negligible, when material characterized by big work hardening exponent and the level of the J -integral is quite large ($J \geq 50\text{kN/m}$). For weakly hardening materials, $Q=Q(T)$ trajectories are parallel, when J -integral characterized by very high level (for example $J=250\text{kN/m}$ or $J=500\text{kN/m}$).

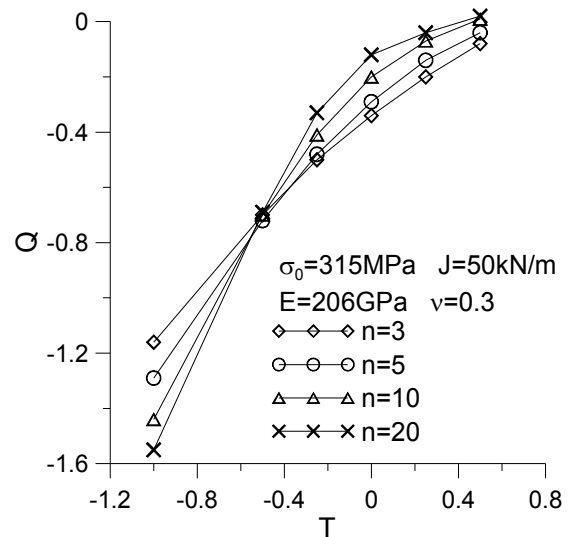


Fig. 10. The influence of the work hardening exponent on the $Q=Q(T)$ trajectories for MBLA characterized by $\sigma_0=315\text{MPa}$, $J=50\text{kN/m}$

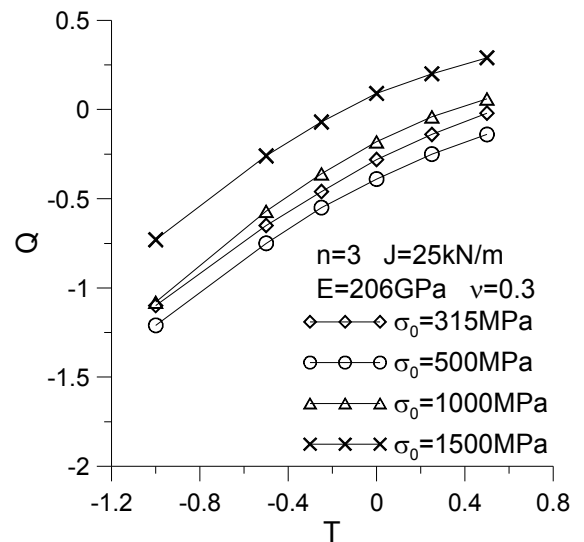


Fig. 11. The influence of the yield stress on the $Q=Q(T)$ trajectories for MBLA characterized by $n=3$, $J=25\text{kN/m}$

The most important conclusion concerns the influence of the J -integral (which is used to determination of the boundary conditions for MBLA model) on Q stress value. As shown by numerical calculations, the value of the Q parameter as a function of the T stress parameter in a very small extent depends on the J -integral value adopted to determine the boundary conditions at MBLA issue. A very little impact (hardly insignificant), or the lack of impact is characterized for MBLA models, for which the J -integral level used to determination of the boundary conditions was equal to or greater than 50kN/m (see Fig. 12).

Fig. 13 presents the influence of the work hardening exponent on Q stress value for different level of the T stress parameter, which may be considered as a measure of the "in-plane constraint" parameter. For the case of low constraints (low value of the T stress, equal to -0.5 or -1.0), Q stress value decreases when the value of the work hardening exponent increases. When the value of the T stress parameter is greater than -0.25 , it can be seen that Q stress value is constant or slightly increases if value of the work hardening exponent increases.

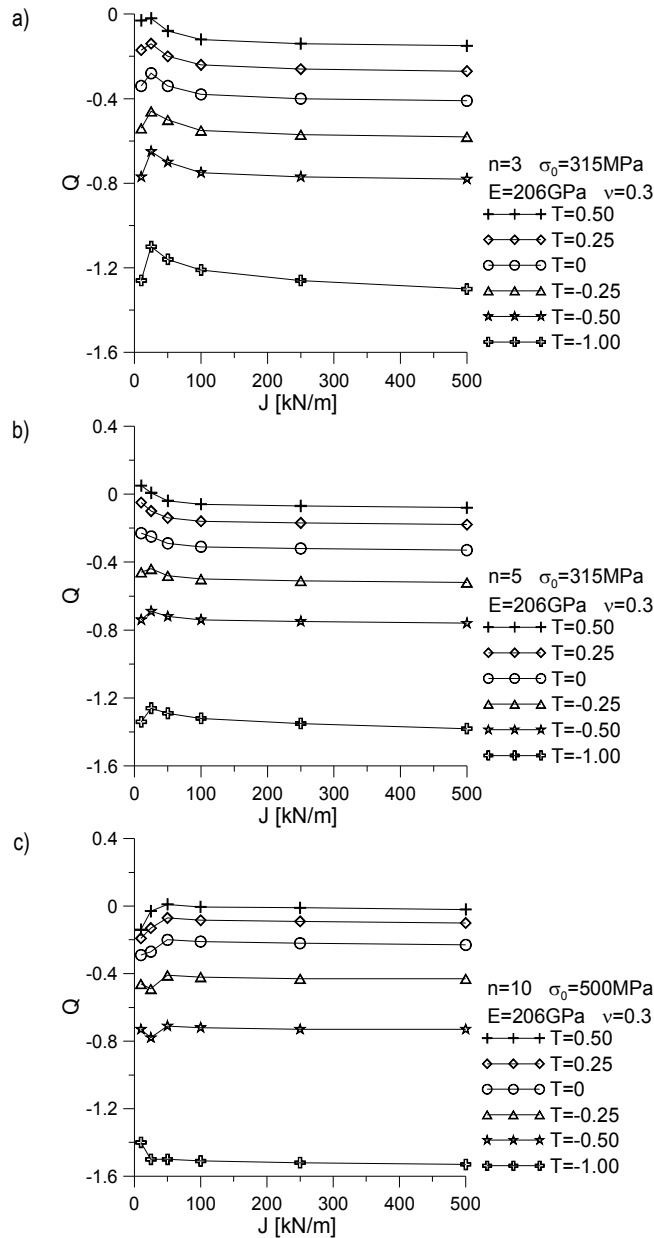


Fig. 12. The influence of the J -integral value which was used to determination of the boundary conditions, on Q stress value for different T stress parameter: a) $n=3$, $\sigma_0=315\text{MPa}$; b) $n=5$, $\sigma_0=315\text{MPa}$; c) $n=10$, $\sigma_0=500\text{MPa}$

5. CONCLUSIONS

In the paper, catalogue of the numerical solutions based on Modify Boundary Layer Approach to determine the relationship between Q -stress and T -stress were presented. Based on method proposed by Larsson and Carlsson, the Q -stress value were calculated for sixteen elastic-plastic materials for different value of T -stress and external load expressed by J -integral – both parameter were used to determine the boundary conditions, which are necessary to carry out the MBLA analysis. The influence of the T -stress parameter and material properties on Q -stress value were tested.

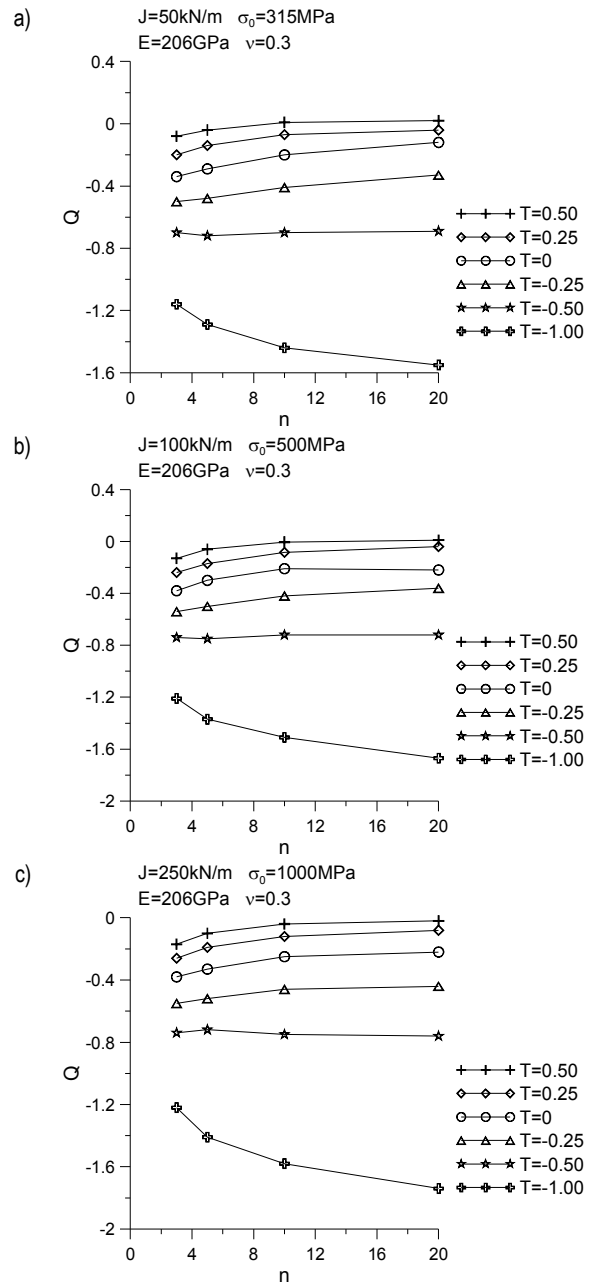


Fig. 13. The influence of the work hardening exponent on Q stress value for different level of the T stress parameter: a) $J=50\text{kJ/m}$, $\sigma_0=315\text{MPa}$; b) $J=100\text{kJ/m}$, $\sigma_0=500\text{MPa}$; c) $J=250\text{kJ/m}$, $\sigma_0=1000\text{MPa}$

Obtained numerical results lead to following conclusions:

- for smaller value of the T stress parameter, the smaller value of the Q stress are observed;
- the influence of yield stress on the Q stress value is significant for the case characterized by low level of the J -integral, adopted to determine the boundary conditions at MBLA issue;
- in case of a higher level of the J -integral, it can be observed a little impact of the yield stress on the Q stress value, sometimes this effect is negligible;
- for different T stress value, Q stress value depends on work hardening exponent n ; this influence should be discussed for each MBLA models separately;
- the Q stress parameter very weak depends (or in general does not depend) on the level of the J -integral adopted

to determine the boundary conditions in MBLA issue, especially for the case when the level of the J -integral is equal to or greater than 50kN/m.

Presented in the paper such catalogue may be useful during solving the engineering problems, especially while is needed to determine real fracture toughness with including the geometric constraints, what was proposed in FITNET procedures (FITNET, 2006).

REFERENCES

1. **ADINA** (2008a), *ADINA 8.5.4: ADINA: Theory and Modeling Guide - Volume I: ADINA*, Report ARD 08-7, ADINA R&D, Inc., 2008.
2. **ADINA** (2008b), *ADINA 8.5.4: ADINA: User Interface Command Reference Manual - Volume I: ADINA Solids & Structures Model Definition*, Report ARD 08-6, ADINA R&D, Inc., 2008.
3. **Ainsworth R.A., O'Dowd N.P.** (1994), A Framework of Including Constraint Effects in the Failure Assessment Diagram Approach for Fracture Assessment, *ASME Pressure Vessels and Piping Conference*, PVP-Vol 287/MD-Vol47, ASME.
4. **Betegon, C. and Hancock, J.W.** (1991), Two Parameter Characterization of Elastic-Plastic Crack Tip Fields, *Journal of Applied Mechanics*, Vol. 58, 104-110.
5. **Bilby, B.A., Cardew, G.E., Goldthorpe, M.R., Howard, I.C.** (1986), A Finite Element Investigation of the Effects of Specimen Geometry on the Fields of Stress and Strain at the Tips of Stationary Cracks, *Size Effects in Fracture*, Institute of Mechanical Engineers, London, 37-46.
6. **FITNET Fitness for Service Procedure – Final Draft** (2006), Edited by M. Koçak, S. Webster, JJ. Janosh, RA. Ainsworth, R. Koers.
7. **Galkiewicz J., Graba M.** (2006), Algorithm for Determination of $\tilde{\sigma}_{ij}(n, \theta)$, $\tilde{\epsilon}_{ij}(n, \theta)$, $\tilde{u}_i(n, \theta)$, $d_n(n)$ and $I_n(n)$ Functions in Hutchinson-Rice-Rosengren Solution and its 3d Generalization, *Journal of Theoretical and Applied Mechanics*, Vol. 44, No. 1, 19-30.
8. **Hutchinson J. W.** (1968), Singular Behaviour at the End of a Tensile Crack in a Hardening Material, *Journal of the Mechanics and Physics of Solids*, 16, 13-31.
9. **Irwin, G.R.** (1957), Analysis of Stresses and Strains near the End of a Crack Traversing a Plate, *Journal of Applied Mechanics*, Vol. 24, 361-364.
10. **Leevers P.S., Radon J.C.** (1983), Inherent Stress Biaxiality in Various Fracture Specimen Geometries, *International Journal of Fracture*, 19, 311-325
11. **McMeeking, R.M. and Parks, D.M.** (1979), On Criteria for J-Dominance of Crack Tip Fields in Large-Scale Yielding, *ASTM STP 668*, American Society for Testing and Materials, Philadelphia, 175-194.
12. **Neimitz A., Graba M., Galkiewicz J.** (2007), An Alternative

Formulation of the Ritchie-Knott-Rice Local Fracture Criterion, *Engineering Fracture Mechanics*, Vol. 74, 1308-1322.

13. **O'Dowd N. P.** (1995), Applications of two parameter approaches in elastic-plastic fracture mechanics, *Engineering Fracture Mechanics*, Vol. 52, No. 3, 445-46.
14. **O'Dowd N. P., Shih C. F.** (1992), Family of Crack-Tip Fields Characterized by a Triaxiality Parameter – II. Fracture Applications, *J. Mech. Phys. Solids*, Vol. 40, No. 5, 939-963.
15. **O'Dowd N. P., Shih C.F.** (1991), Family of Crack-Tip Fields Characterized by a Triaxiality Parameter – I. Structure of Fields, *J. Mech. Phys. Solids*, Vol. 39, No. 8, 989-1015.
16. **Rice J. R., Rosengren G. F.** (1968), Plane Strain Deformation Near a Crack Tip in a Power-law Hardening Material, *Journal of the Mechanics and Physics of Solids*, 16, 1-12.
17. **Rice, J.R.** (1968), A Path Independent Integral and the Approximate Analysis of Strain Concentration by Notches and Cracks, *Journal of Applied Mechanics*, Vol. 35, pp. 379-386.
18. **Sherry A.H., Hooton D.G., Beardsmore D.W., Lidbury D.P.G.** (2005), Material constraint parameters for the assessment of shallow defects in structural components – Part II: constraint – based assessment of shallow cracks, *Engineering Fracture Mechanics*, 72, 2396-2415.
19. **Sherry A.H., France C.C., Goldthorpe M.R.** (1995), Compendium of T-stress solutions for two and three dimensional cracked geometries, *Fatigue & Fracture of Engineering Materials & Structures*, Vol. 18, No. 1, 141-155.
20. **Sherry, A.H., Wilkes M.A., Beardsmore D.W., Lidbury D.P.G.** (2005), Material constraint parameters for the assessment of shallow defects in structural components – Part I: Parameter solutions, *Engineering Fracture Mechanics*, 72, 2373-2395.
21. **SINTAP** (1999), *SINTAP: Structural Integrity Assessment Procedures for European Industry. Final Procedure*, Brite-Euram Project No BE95-1426. – Rotherham: British Steel.
22. **Sneddon, I.N.** (1946), The Distribution of Stress in the Neighbourhood of a Crack in an Elastic Solid, *Proceedings*, Royal Society of London, Vol. A-187, 229-260.
23. **Sumpter J. G. D., Forbes A. T.** (1992), Constraint based analysis of shallow cracks in mild steels, *Proceedings of TWI/EWI/IS Int. Conf on Shallow Crack Fracture Mechanics, Toughness Tests and Applications*, Paper 7, Cambridge U.K.
24. **Westergaard, H.M.** (1939), Bearing Pressures and Cracks, *Journal of Applied Mechanics*, Vol. 6, 49-53.
25. **Williams, M.L.** (1957), On the Stress Distribution at the Base of a Stationary Crack, *Journal of Applied Mechanics*, Vol. 24, 109-114.

Acknowledgments: The support of the Kielce University of Technology – Faculty of Mechatronics and Machine Design through grant No 1.22/7.14 is acknowledged by the author of the paper.

ANNEX - NUMERICAL RESULTS OBTAINED FOR ALL MBLA MODELS

Tab. A.1. Results for MBLA models, characterized by $J=10\text{kN/m}$

$J=10\text{kN/m}$ $\sigma=315\text{MPa}$	n			
	3	5	10	20
T	Q			
0.50	-0.03	0.05	0.05	0.02
0.25	-0.17	-0.05	-0.01	-0.02
0	-0.34	-0.23	-0.16	-0.15
-0.25	-0.54	-0.46	-0.4	-0.39
-0.50	-0.77	-0.74	-0.73	-0.76
-1.00	-1.26	-1.34	-1.47	-1.65

$J=10\text{kN/m}$ $\sigma=500\text{MPa}$	n			
	3	5	10	20
T	Q			
0.50	0.29	0.04	-0.14	-0.23
0.25	0.18	-0.04	-0.19	-0.27
0	0.05	-0.17	-0.29	-0.36
-0.25	-0.12	-0.35	-0.46	-0.53
-0.50	-0.31	-0.58	-0.73	-0.81
-1.00	-0.74	-1.11	-1.40	-1.63

J=10kN/m σv=1000MPa	n			
	3	5	10	20
T	Q			
0.50	0.46	0.1	-0.17	-0.30
0.25	0.39	0.04	-0.19	-0.31
0	0.30	-0.04	-0.25	-0.34
-0.25	0.19	-0.16	-0.36	-0.43
-0.50	0.05	-0.33	-0.54	-0.63
-1.00	-0.29	-0.78	-1.16	-1.39
J=10kN/m σv=1500MPa	n			
	3	5	10	20
T	Q			
0.50	0.4	0.12	-0.07	-0.17
0.25	0.36	0.07	-0.11	-0.20
0	0.29	-0.01	-0.18	-0.26
-0.25	0.2	-0.13	-0.3	-0.36
-0.50	0.08	-0.28	-0.48	-0.56
-1.00	-0.21	-0.70	-1.07	-1.28

Tab. A.2. Results for MBLA models, characterized by J=25kN/m

J=25kN/m σv=315MPa	n			
	3	5	10	20
T	Q			
0.50	-0.02	0.007	0.04	0.04
0.25	-0.14	-0.10	-0.03	-0.01
0	-0.28	-0.25	-0.17	-0.15
-0.25	-0.46	-0.44	-0.38	-0.35
-0.50	-0.65	-0.69	-0.69	-0.70
-1.00	-1.10	-1.26	-1.43	-1.60
J=25kN/m σv=500MPa	n			
	3	5	10	20
T	Q			
0.50	-0.14	-0.09	-0.03	0.008
0.25	-0.25	-0.2	-0.13	-0.09
0	-0.39	-0.34	-0.27	-0.24
-0.25	-0.55	-0.53	-0.49	-0.48
-0.50	-0.75	-0.77	-0.78	-0.83
-1.00	-1.21	-1.36	-1.50	-1.66
J=25kN/m σv=1000MPa	n			
	3	5	10	20
T	Q			
0.50	0.06	0.03	-0.02	-0.07
0.25	-0.04	-0.07	-0.08	-0.11
0	-0.18	-0.21	-0.21	-0.23
-0.25	-0.36	-0.42	-0.44	-0.46
-0.50	-0.57	-0.69	-0.75	-0.80
-1.00	-1.08	-1.35	-1.59	-1.78
J=25kN/m σv=1500MPa	n			
	3	5	10	20
T	Q			
0.50	0.29	0.04	-0.16	-0.27
0.25	0.20	-0.03	-0.20	-0.29
0	0.09	-0.14	-0.29	-0.37

-0.25	-0.07	-0.31	-0.46	-0.53
-0.50	-0.26	-0.54	-0.72	-0.80
-1.00	-0.73	-1.13	-1.48	-1.7

Tab. A.3. Results for MBLA models, characterized by J=50kN/m

J=50kN/m σv=315MPa	n			
	3	5	10	20
T	Q			
0.50	-0.08	-0.04	0.009	0.02
0.25	-0.20	-0.14	-0.07	-0.04
0	-0.34	-0.29	-0.20	-0.12
-0.25	-0.50	-0.48	-0.41	-0.33
-0.50	-0.70	-0.72	-0.70	-0.69
-1.00	-1.16	-1.29	-1.44	-1.55
J=50kN/m σv=500MPa	n			
	3	5	10	20
T	Q			
0.50	-0.10	-0.04	0.01	0.02
0.25	-0.22	-0.15	-0.07	-0.12
0	-0.35	-0.29	-0.20	-0.23
-0.25	-0.52	-0.48	-0.41	-0.37
-0.50	-0.72	-0.73	-0.71	-0.72
-1.00	-1.19	-1.35	-1.50	-1.34
J=50kN/m σv=1000MPa	n			
	3	5	10	20
T	Q			
0.50	-0.16	-0.10	-0.05	-0.01
0.25	-0.25	-0.19	-0.13	-0.09
0	-0.38	-0.33	-0.28	-0.25
-0.25	-0.54	-0.52	-0.50	-0.49
-0.50	-0.74	-0.77	-0.79	-0.82
-1.00	-1.22	-1.40	-1.58	-1.73
J=50kN/m σv=1500MPa	n			
	3	5	10	20
T	Q			
0.50	-0.09	0.02	0.08	0.08
0.25	-0.19	-0.08	0.001	0.02
0	-0.32	-0.24	-0.16	-0.13
-0.25	-0.50	-0.46	-0.40	-0.39
-0.50	-0.72	-0.74	-0.75	-0.76
-1.00	-1.25	-1.45	-1.66	-1.82

Tab. A.4. Results for MBLA models, characterized by J=100kN/m

J=100kN/m σv=315MPa	n			
	3	5	10	20
T	Q			
0.50	-0.12	-0.06	-0.004	0.01
0.25	-0.24	-0.16	-0.08	-0.04
0	-0.38	-0.31	-0.22	-0.16
-0.25	-0.55	-0.50	-0.42	-0.36
-0.50	-0.75	-0.74	-0.72	-0.70
-1.00	-1.21	-1.32	-1.46	-1.61

J=100kN/m $\sigma_v=500\text{MPa}$	n			
	3	5	10	20
T	Q			
0.50	-0.13	-0.06	-0.005	0.01
0.25	-0.24	-0.17	-0.084	-0.04
0	-0.38	-0.30	-0.21	-0.22
-0.25	-0.54	-0.50	-0.42	-0.36
-0.50	-0.74	-0.75	-0.72	-0.72
-1.00	-1.21	-1.37	-1.51	-1.67
J=100kN/m $\sigma_v=1000\text{MPa}$	n			
	3	5	10	20
T	Q			
0.50	-0.15	-0.08	-0.03	-0.006
0.25	-0.23	-0.17	-0.10	-0.06
0	-0.36	-0.30	-0.23	-0.19
-0.25	-0.52	-0.50	-0.45	-0.42
-0.50	-0.72	-0.75	-0.74	-0.75
-1.00	-1.20	-1.40	-1.57	-1.74
J=100kN/m $\sigma_v=1500\text{MPa}$	n			
	3	5	10	20
T	Q			
0.50	-0.13	-0.08	-0.04	-0.02
0.25	-0.20	-0.16	-0.11	-0.09
0	-0.32	-0.30	-0.26	-0.23
-0.25	-0.48	-0.50	-0.47	-0.46
-0.50	-0.67	-0.74	-0.76	-0.78
-1.00	-1.15	-1.38	-1.60	-1.76

Tab. A.5. Results for MBLA models, characterized by J=250kN/m

J=250kN/m $\sigma_v=315\text{MPa}$	n			
	3	5	10	20
T	Q			
0.50	-0.14	-0.07	-0.01	0.008
0.25	-0.26	-0.17	-0.08	-0.05
0	-0.40	-0.32	-0.22	-0.15
-0.25	-0.57	-0.51	-0.43	-0.38
-0.50	-0.77	-0.75	-0.72	-0.72
-1.00	-1.26	-1.35	-1.47	-1.62
J=250kN/m $\sigma_v=500\text{MPa}$	n			
	3	5	10	20
T	Q			
0.50	-0.16	-0.08	-0.01	0.004
0.25	-0.27	-0.18	-0.09	-0.05
0	-0.40	-0.32	-0.22	-0.17
-0.25	-0.57	-0.51	-0.43	-0.38
-0.50	-0.77	-0.76	-0.73	-0.71
-1.00	-1.26	-1.39	-1.52	-1.68
J=250kN/m $\sigma_v=1000\text{MPa}$	n			
	3	5	10	20
T	Q			
0.50	-0.17	-0.1	-0.04	-0.02
0.25	-0.26	-0.19	-0.12	-0.08
0	-0.38	-0.33	-0.25	-0.22

-0.25	-0.55	-0.52	-0.46	-0.44
-0.50	-0.74	-0.72	-0.75	-0.76
-1.00	-1.22	-1.41	-1.58	-1.74
J=250kN/m $\sigma_v=1500\text{MPa}$	n			
	3	5	10	20
T	Q			
0.50	-0.19	-0.14	-0.08	-0.06
0.25	-0.27	-0.22	-0.16	-0.13
0	-0.38	-0.35	-0.30	-0.27
-0.25	-0.54	-0.54	-0.50	-0.49
-0.50	-0.73	-0.78	-0.79	-0.80
-1.00	-1.20	-1.40	-1.61	-1.77

Tab. A.6. Results for MBLA models, characterized by J=500kN/m

J=500kN/m $\sigma_v=315\text{MPa}$	n			
	3	5	10	20
T	Q			
0.50	-0.15	-0.08	-0.01	0.005
0.25	-0.27	-0.18	-0.09	-0.05
0	-0.41	-0.33	-0.23	-0.17
-0.25	-0.58	-0.52	-0.43	-0.38
-0.50	-0.78	-0.76	-0.73	-0.73
-1.00	-1.30	-1.38	-1.47	-1.50
J=500kN/m $\sigma_v=500\text{MPa}$	n			
	3	5	10	20
T	Q			
0.50	-0.17	-0.09	-0.02	0.002
0.25	-0.28	-0.19	-0.10	-0.05
0	-0.41	-0.33	-0.23	-0.17
-0.25	-0.58	-0.52	-0.43	-0.38
-0.50	-0.78	-0.77	-0.73	-0.72
-1.00	-1.29	-1.42	-1.53	-1.62
J=500kN/m $\sigma_v=1000\text{MPa}$	n			
	3	5	10	20
T	Q			
0.50	-0.19	-0.12	-0.05	-0.03
0.25	-0.28	-0.21	-0.13	-0.09
0	-0.40	-0.34	-0.26	-0.22
-0.25	-0.56	-0.53	-0.47	-0.45
-0.50	-0.76	-0.78	-0.76	-0.77
-1.00	-1.25	-1.43	-1.59	-1.75
J=500kN/m $\sigma_v=1500\text{MPa}$	n			
	3	5	10	20
T	Q			
0.50	-0.23	-0.16	-0.1	-0.08
0.25	-0.30	-0.24	-0.18	-0.14
0	-0.42	-0.38	-0.32	-0.28
-0.25	-0.57	-0.56	-0.53	-0.50
-0.50	-0.76	-0.80	-0.80	-0.82
-1.00	-1.23	-1.43	-1.62	-1.78